Laser and optical properties of Yb:YAG ceramics with layered doping distribution: design, characterization and evaluation of different production processes

Guido Toci*[a], Antonio Lapucci[b], Marco Ciofini[b], Laura Esposito[c], Jan Hostaša[c], Leonida Antonio Gizzi[d], Luca Labate[d], Paolo Ferrara[d], Angela Pirri[e], Matteo Vannini[a]

[a] CNR – INO National Research Council, National Institute of Optics, Via Madonna del Piano 10, I-50019 Sesto Fiorentino (FI) Italy

[b] CNR - INO National Research Council, National Institute of Optics, Largo Enrico Fermi 6, I-50125 Firenze, Italy

[c] CNR - ISTEC National Research Council, Institute of Science and Technology for Ceramics, Via Granarolo 64, 48018 Faenza, Italy

[d] CNR - INO National Research Council, National Institute of Optics, Via G. Moruzzi, 1, I-56124 Pisa, Italy

[e] CNR - IFAC National Research Council, Institute of Applied Physics "Nello Carrara", Via Madonna del Piano 10, I-50019 Sesto Fiorentino (FI) Italy

ABSTRACT

The laser, optical and spectroscopic properties of multilayer Yb:YAG ceramic structures, differently activated, were investigated. The structures were designed by means of Finite Element Modeling, adjusting the doping distributions to reduce peak temperature, surface deformation and thermally induced stresses, depending on the pump and cooling geometry.

Two ceramic processes were used, i.e. dry pressing of spray-dried powders (SD) and tape casting (TC), resulting in different defect density and size distribution: TC gives a more uniform transmission, whereas SD results in larger, unevenly scattered defects. The spectroscopic properties were found independent from the production process.

The laser performance has been characterized under high intensity pumping in a longitudinally diode pumped laser cavity, comparing the behavior of the different structures in terms of slope efficiency, stability under increasing thermal load, spatial uniformity of laser emission. Slope efficiency values as high as 58% in Quasi-CW pumping conditions and 54% in CW conditions was measured in two-layers structures. The production process and the number of layers influenced the behavior of the samples, in particular regarding the spatial uniformity of the laser emission. Samples made by tape casting have shown overall a better thermal stability with respect to the samples made by spray drying.

Keywords: YAG; Transparent ceramics; Laser; Thermal effects; Multilayer ceramics; Yb lasers.

1. INTRODUCTION

The last decade has witnessed a steadily growing interest on two specific fields of laser physics and technology: the development of Yb doped solid state materials, and the development of transparent polycrystalline ceramics for laser applications. The success of Yb as a dopant for solid state laser materials is motivated by the occurrence of several interesting features that make it suitable for high power and high efficiency laser devices [1],[2]. Moreover the large availability of hosts for Yb^{3+} feeds a broad variability in the spectroscopic, optical and thermomechanical properties, which allows a fine optimization of the material parameters for specific applications. The availability of new hosts for Yb is further widened by the development of transparent polycrystalline ceramics, which provide unique advantages with respect to the fabrication of single crystals. The continuous improvement in the fabrication techniques allowed to obtain a high level of transparency, currently comparable with high quality conventional crystals, and a strong reduction of scattering due to internal defects, which affected the laser performances in the first experiments. The ceramic fabrication methods usually require lower processing temperatures than crystal growth techniques: this enables or ease the fabrication of materials which, due to the high melting point, are difficult to fabricate with crystal growth technique,

Solid State Lasers XXV: Technology and Devices, edited by W. Andrew Clarkson, Ramesh K. Shori, Proc. of SPIE Vol. 9726, 97261P · © 2015 SPIE · CCC code: 0277-786X/15/$18 · doi: 10.1117/12.2211344

as in the case of sesquioxides and some garnets [3],[4]. The microstructure of polycrystalline ceramics can also result in a higher mechanical resistance [[5] with respect to single crystals.

Ceramic laser materials can also offer peculiar advantages in the development of high power or high energy laser devices. In particular, ceramic gain elements can be fabricated with large size and apertures, more easily and rapidly than single crystals.

Finally, the ceramic fabrication processes allow a tight control in the dopants distribution inside the active element [6], making it possible to obtain gain elements with specifically tailored, non uniform dopant distribution inside the gain element, or even to introduce of different dopants in various region of the same composite element, with a minimal number of fabrication steps. These features are much more difficult to obtain with crystal technologies.

The control in the distribution of the dopant can be successfully exploited to manage and reduce the thermal effects (TEs) and thermo-mechanical effects (TMEs) (*e.g.* thermal lens, stress-induced depolarization, surface deformations) deriving from the laser pumping process. These effects can degrade the performance of the laser source and can eventually lead to a catastrophic failure of the laser active element, in particular when high pumping power densities are employed. Moreover, in the case of Yb YAG the temperature increase modify the spectroscopic properties of the lasing levels, leading to an overall reduction of the laser efficiency [[7]. Finally, a suitable, non uniform dopant distribution can help to reduce Amplified Spontaneous Emission (ASE) effects with respect to an uniform doping [8].

In this paper, we report on the design and the characterization of the optical, spectroscopic and laser emission properties of multi-layer Yb:YAG ceramic gain elements with one-dimensional Yb dopant distribution. The dopant distribution was designed by means of Finite Elements Analysis (FEM) for the evaluation of the thermal and thermomechanical behavior resulting in an end-pumped, end-cooled configuration, with the aim to reduce the peak temperature and the surface deformation with respect to an uniform dopant distribution which has the same overall gain.

The sample under test were fabricated with two different fabrication methods, namely cold pressing of spray dried powders and tape casting, which are described in details in another paper in these Proceedings [9]. We have compared the characteristics of the samples obtained with these two methods, obtaining clear indications for further developments.

2. THERMOMECHANICAL ANALYSIS OF MULTILAYER ELEMENTS

The thermal and thermo-mechanical behavior of ceramics elements with layered doping distributions was analyzed by means of several numerical simulations based on FEM, using a commercial package (COSMOS [10]). The details of the modeling method were described in a previous publication, and are summarized here for convenience [11]. The simulation was conducted using heat loading distributions and thermal boundary conditions similar to the experiment reported later in this paper. In particular we have analyzed two different Yb doping distributions:

a) stepped (0-10%) with thickness of the layers 1.2mm-1.8 mm
b) graded (3-5-7%) with thickness of the layers 1.2 mm-1.2 mm-0.6 mm respectively.

The results on thermomechanical behavior of these two structures were compared with those of two homogeneous elements with the same thickness of the doped layer(s) and the same overall pump absorption, namely an homogeneous element with 10% doping and 1.8 mm thickness as a paragon for the stepped doping distribution, and an homogeneous element with 5% doping with a thickness of 3 mm in comparison with the structure with graded doping.

Our software package output consists in a scalar temperature variation field $\Delta T=T- T_{REF}$, the geometrical displacements of each node of the mesh and, finally, the 6 components of the stress tensor (σ_i and τ_{ij}). These data give an immediate information on some operational features of the different samples as laser active media. The maximum internal stress at a given power loading is, for instance, an indicator of how far we are working from the "fracture limit". Furthermore they can be used to calculate thermo-optical effects such as thermal lens or stress induced depolarization.
The pump beam was considered to have a top hat intensity distribution, with a diameter of 500 μm. The sample is conductively cooled on the opposite side (with respect to the pumping side), on an outer with internal diameter of 5 mm centered on the pump beam axis. The overall diameter of the samples is 10 mm. In each point of the pumped volume the thermal load (thermal dissipation for unit volume) is considered proportional to the absorbed power density (watt/m^3). The pump absorption constant was calculated considering the pumping wavelength at 940 nm. The overall power dissipation was kept constant at 2.65 W for all the doping distributions under investigation. Differently from Ref. [11]

the thermal conductivity of the material for each doping level was calculated as a function of the Yb concentration using the model provided by Gaume [12]. The material parameters used int he simulation are resumed in Table 1.

Table 1. Thermomechanical parameters of Yb:YAG used in the simulations.

Doping	Absorption constant (cm^{-1})	Thermal conductivity (W/(mK))	Thermal expansion coefficient (1/K)	Young modulus (Pa)	Poisson number
0%	0.0	10.7	8×10^{-6}	0.280×10^{12}	0.28
3%	1.5	9.8			
5%	2.5	8.4			
7%	3.5	8.2			
10%	10.0	6.7			

The pictures below (Figure 1) shows the internal temperature distribution on a diametral plane for the sample with stepped doping distribution, in comparison with its reference sample (10% uniform doping). In the case of the two-layers sample, the pump beam enters in the sample from the undoped side. The temperature of the heat sink is set at 20 °C.

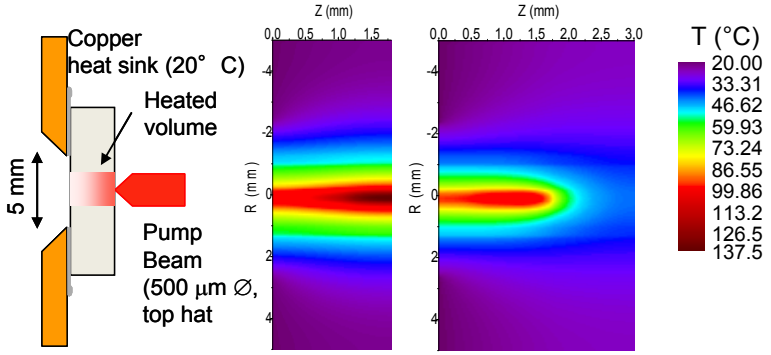

Figure 1. Left: schematics of the pumping and cooling geometry used in the simulations. A diametral cross section of the sample is shown, evidencing the incidence direction of the pump beam and of the heat sink. Center: temperature distribution of an uniform sample with 1.8 mm thickness and 10% Yb doping. Right: temperature distribution of a two-layers sample with the undoped layer on the side of incidence of the pump beam. The color scale is the same for both figures. Color online.

It can be seen that the peak temperature in the stepped sample is significantly lower than in the case of the uniformly doped sample, by about 30 °C, because the undoped layer on the pump incidence side acts as a spreader for the heat generated in the doped layer by the pump absorption. As the undoped layer is not directly heated by the pump beam (but only by conduction of the heat generated in the nearby doped layer) it is also much less subjected to thermal expansion and deformation, and it limits the bulging of the underlying doped layer with respect to the homogeneously doped sample. This is exemplified in Figure 2, which shows the deformation of the sample (assuming a rigid and non-slipping boundary condition on the part in contact with the heat sink). It can be seen that the deformation of the two layers sample in the central part is significantly smaller (about 25% less) than the deformation of the homogeneous sample, in particular on the undoped side. This implies that the surfaces of the two-layers sample are subjected to a lower tensile stress in the directions parallel to te surface itself, reducing the risk of rupture for thermomechanical stress.

The results for the sample with graded doping distribution are shown in Figure 3 and Figure 4. It can be seen that the non uniform distribution of the doping reallocates the thermal load distribution, resulting in a more smooth longitudinal temperature profile and in a reduction of the peak temperature. The reduction of the peak temperature near to the surface also produces a reduction in the overall deformation of the samples as in the previous case, as it is shown in Figure 4.

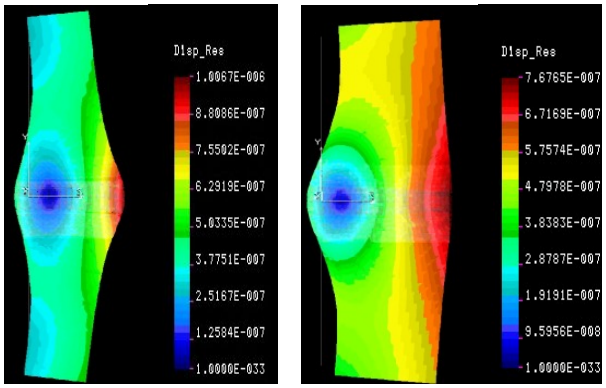

Figure 2. Distribution of displacements (in meters) of the samples samples with homogeneous doping and stepped doping. Left: displacements for the sample with homogeneous doping; right: displacements for the sample with two layers. Please note that the color scale is not the same for the two figures. Color online.

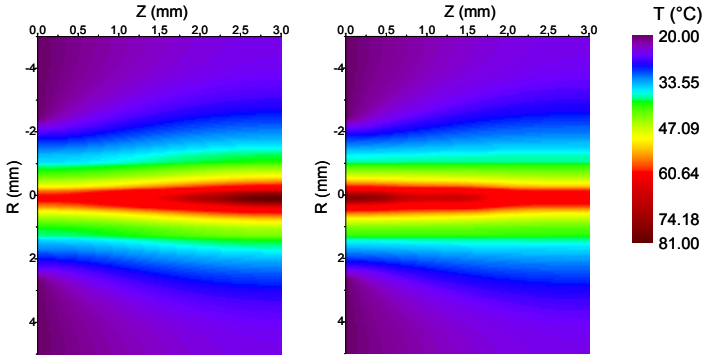

Figure 3. Left: temperature distribution of an uniform sample with 3.0 mm thickness and 5% Yb doping. Right: temperature distribution of a three layers sample with doping 3%-5%-7%. The arrangement of the pump beam and of the heat sink is the same shown in Figure 1. The side with the lowest doping is facing the pump incidence direction. The color scale is the same for both figures. Color online.

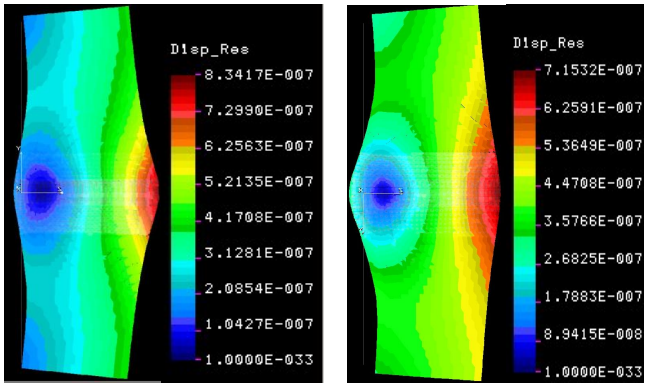

Figure 4. Distribution of displacements (in meters) of the two samples with homogeneous doping and graded doping. Left: displacements for the sample with homogeneous doping; right: displacements for the sample with two layers. Please note that the color scale is not the same for the two figures. Color online.

3. SPECTROSCOPIC AND OPTICAL CHARACTERIZATION

Sample preparation

Yb:YAG ceramic samples with non uniform doping distribution were prepared using two different techniques, namely cold pressing of spray dried powers and hot pressing of tape cast layers (heretofore SD and TC respectively), followed by reactive sintering. A detailed description of the two fabrication techniques, as well as an in-depth microstructural characterization are reported in another paper of these Proceedings [9]. In summary, both processes start from high purity Al_2O_3 Y_2O_3 Yb_2O_3 with micrometric or nanometric size, and ball milled for several hours with suitable solvents. and sintering aids; in the case of the tape casting procedure, organic adhesive additives are added; the slurry is then cast in sheets of about 100 μm thickness. Disks with a diameter of 40 mm were cut from the sheets and assembled together, with the required Yb content sequence. The resulting disks stacks are then thermally compressed at 100°C; during the thermal compression the heat softens the organic additives promoting the adhesion of disks. The organic additives are then removed by calcination in air at 600°C. Finally sintering was conducted under high vacuum in a clean, carbon-free furnace at 1730°C x 16 hours.

In the case of the spray drying process, after the ball milling the slurries were granulated by spray drying. Pellets 15 mm in diameter and about 1 mm thick were then obtained by separate uniaxial pressing of each granulated powders. The layered samples were prepared by (linear and cold isostatic) pressing of the thin pellets appropriately assembled to obtain the required doping distribution, followed by the calcination and the reactive sintering phases as in the tape cast process.

The doping levels and the layer thicknesses of the samples included in this investigation are reported in Table 2.

Table 2. Parameters of the samples used in the experiments.

Sample n.	Yb doping %*at.*	Fabrication technique	Total thickness (mm)	Individual layers thickness (mm)
SD-1	0-10	Cold pressing of spray dried powders	3.4	1.5 (Undoped) 1.9 (10 at % Yb)
SD-2	1-3-5-7	Cold pressing of spray dried powders	2.0	0.5
TC-1	0-10	Tape casting and thermal compression	1.9	1.0 (Undoped) 0.9 (10 at % Yb)
TC-2	1-3-5-7	Tape casting and thermal compression	2.0	0.5

Spectroscopic characterization

Transmission spectra of the samples were acquired with a Perkin Elmer Lambda 1050 spectrometer, and are shown in Figure 5. It can be seen that the baseline transmission of the sample TC-1 is much better than the other three samples, whereas the sample SD-2 shows significant scattering losses. The region between 900 and 1050 nm of the transmission spectra of doped samples is obviously dominated by the presence of the absorption of the dopant Yb^{3+}. In addition, the Yb^{3+} is also responsible for the strong absorption for wavelengths smaller than 250 nm due to the absorption of so-called Charge Transfer Transition (CTT) (see e.g. [13]). From the measurements of Figure 5, taking into account the Fresnel reflection at the interfaces and the different thickness of the samples we calculated the average scattering coefficient in the spectral interval 1060-1100 nm. The results are shown in Table 3. It can be seen that the two-layers samples (TC-1 and SD-1) show a similar low value of the scattering coefficient, which is higher in the case of the two multi-layers samples TC-2 and SD-2. Finally, it can be seen that the sample TC-2 shows a broad absorption band in the red (with a peak at about 640 nm) due to a residual presence of Yb^{2+} (see e.g. [14]).

Table 3. Internal transmission and scattering coefficient of the samples used in the experiments.

Sample	Internal transmission (%)	Scattering coefficient α_s (cm^{-1})
SD-1	89.5%	0.32
SD-2	84.7%	0.92
TC-1	94.9%	0.29
TC-2	87.7%	0.73

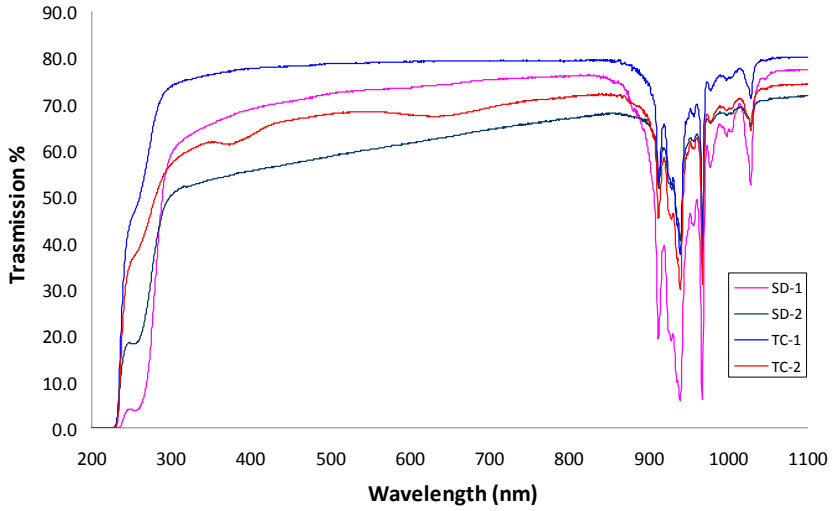

Figure 5. Transmission of the samples described in Table 2. Color online.

The fluorescence spectra of the samples were excited with a semiconductor laser emitting at 936 nm, using a 90° excitation-detection geometry on the sample edge to minimize the reabsorption effects, and acquired with a grating spectrometer equipped with a CCD array. Pulsed excitation and delayed synchronous detection were used to reject the pump signal. The lifetime of the upper laser level was measured using the so-called pinhole method [15] with an experimental set-up described elsewhere [16], to avoid radiation trapping effects. In all the samples the upper level lifetime resulted comprised between 940 and 970 μsec, near to the commonly accepted value of 951 μsec for Yb:YAG [17]. From the fluorescence spectra we calculated the emission cross section spectra using the so-called β-τ method [18]. The spectrum of the emission cross section is shown in Figure 6. The emission spectrum was the same for all the samples and it is consistent with those previously reported in literature for Yb^{3+} in YAG (see for instance [19]).

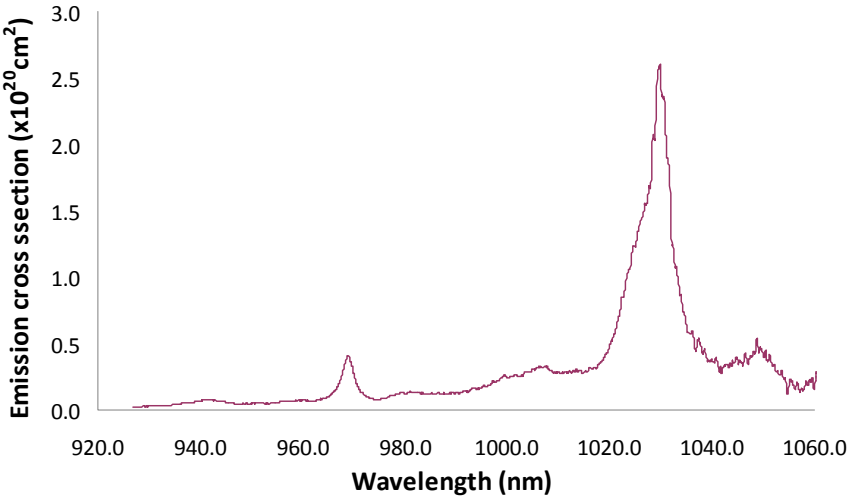

Figure 6. Emission cross section spectrum of the Yb:YAG ceramics.

Optical uniformity mapping

One of the most relevant aspects in the preparation of ceramics for laser applications is the uniformity of the optical properties, and in particular the transmission. Internal pores or localized secondary phases can originate scattering centers and localized nonuniformities in the refractive index. To investigate this subject, we set up a system to obtain the point-by-point mapping of the transmission uniformity of the samples. The experimental set-up is shown in Figure 7.

A probe beam is generated by a He-Ne laser and focused on the sample on a spot with a diameter of about 30 μm. The power of the transmitted beam is measured by a photodiode, whereas a portion of the incident beam is monitored by a reference photodiode. The transmission of the sample in the probed point is calculated by the ratio of the reference and of the transmitted beam power levels. The probe beam is modulated by a chopper to improve the S/N ratio. The resulting accuracy in the measurement of transmission is about 0.3% (2σ). The sample is mounted on a two axis motorized stage, with a resolution of 1 μm, used to scan the relative position of the sample on the beam path in order to obtain the transmission mapping.

Figures 8 shows the transmission maps of the two-layers samples SD-1 and TC-2; the transmission maps of the samples SD-2 and TC-2 with graded doping are shown on Figure 9.

From the comparison of the picture in Figure 8 and 9 (which all have the same color scale) it can be seen that the tape cast process results overall in a lower density of internal defects and in a better background transmission with respect to the spray drying process. This is true both for the samples with stepped doping profile and with graded doping profile. Moreover, the samples with graded doping profile tend to have a larger number of defects than the samples with stepped doping profile. This probably depends from the fact that the samples with graded doping are composed by the assembly of a larger number of layers than the samples with stepped doping, which lead to the formation of an overall larger defect density at the layers interfaces. In the case of the sample TC-2 the transmission at the probe wavelength of 632 nm is slightly reduced by the absorption of the residual Yb^{2+} (see Figure 5).

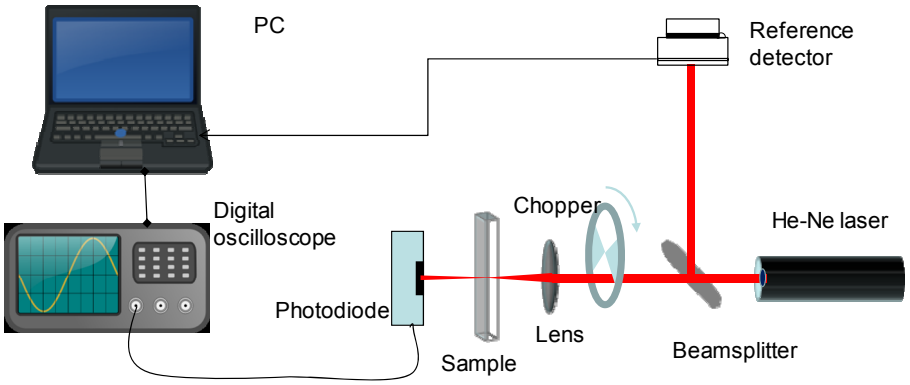

Figure 7. Set up used for the mapping of the uniformity of the ceramic samples.

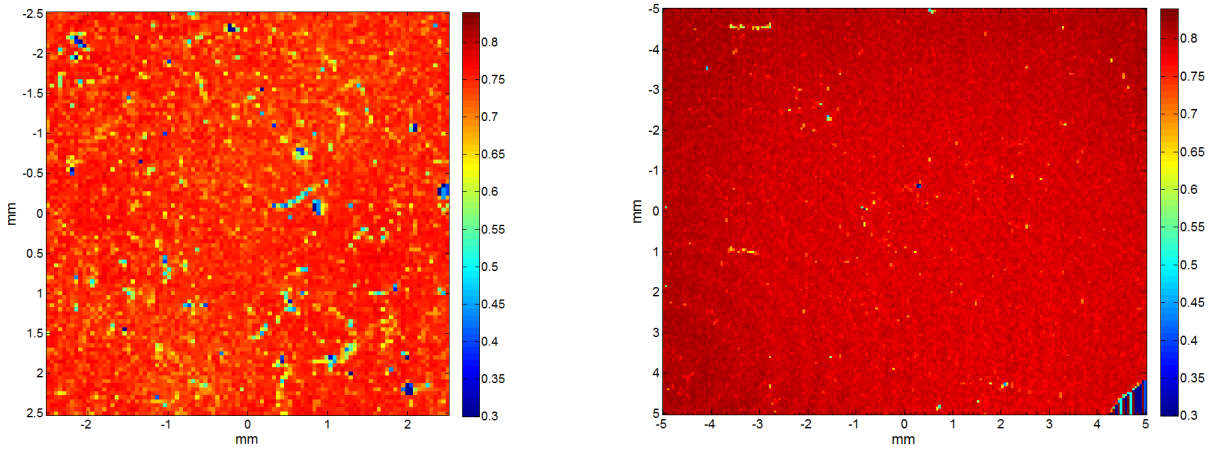

Figure 8. Transmission map of the samples SD-1 (left) and TC-1 (right). The dark area in the lower right corner of the sample TC-1 is due to a missing chip. Color scale is the same for both figures. Color online.

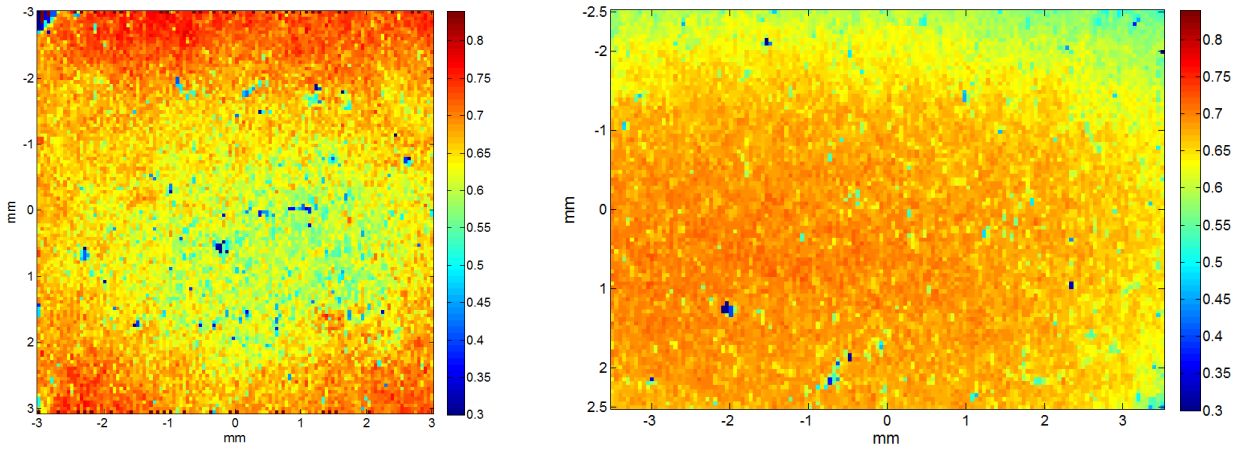

Figure 9. Transmission map of the samples SD-2 (left) and TC-2 (right). Color scale is the same for both figures. Color online.

The comparison of the uniformity of the samples can be made more quantitative by calculating, from the data of Figure 8 and Figure 9, the transmission probability density P(T), so as P(T)ΔT is the probability to have a transmission comprised between T and T+ΔT. The result of this analysis is shown in Figure 10. It can be seen that the sample TC-1 has the highest expectance value for the transmission (peak of the probability density curve) as well as the most uniform transmission (width of the main peak). These characteristics gradually worsen going through the sample SD-1, TC-2 to the sample SD-2.

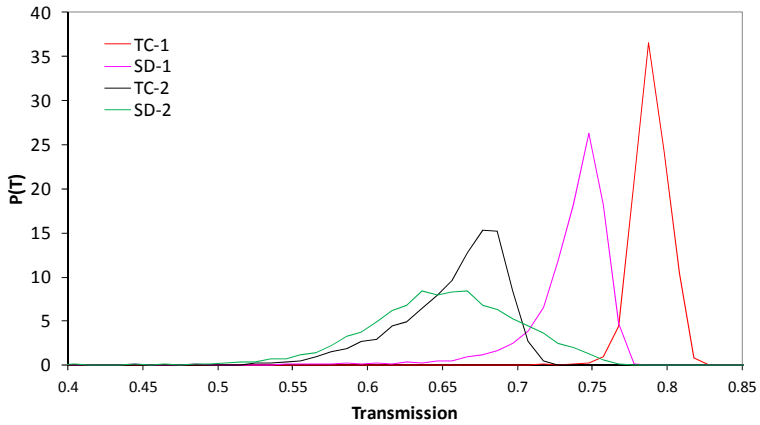

Figure 10. Probability density P(T) versus the value of transmission T determined from the transmission maps of Figure 9 and 10. Color online.

4. CHARACTERIZATION OF THE LASER PROPERTIES

The laser emission properties of the samples under test were characterized in an end-pumped laser cavity. The layout of the laser cavity is shown in Figure 11. The cavity is longitudinally pumped through its flat end mirror EM, which is dichroic with a high transmission at the pump wavelength and a high reflection at the lasing wavelengths.

As a pump source we used a fiber coupled diode laser emitting at 936 nm, with a fiber core diameter of 200 microns and numerical aperture 0.22. The fiber output was refocused into the sample by a pair of achromatic doublets, through the cavity end mirror. The maximum pump power delivered to the sample was about 21W. The pump beam had an almost Gaussian profile with a diameter of 260 μm @ 1/e2 of the peak intensity. The cavity was V-shaped, with a folding mirror FM having a curvature radius of 100 mm set at a small incidence angle, and a flat output coupler OC. The lengths of the cavity arms were D1=62 mm and D2=260 mm respectively. The samples were uncoated, and they were carefully

oriented so as to reinject the Fresnel reflection at the surfaces back on the cavity axis, in order to minimize reflection losses. The samples were placed very near to the EM (less than 1 mm between the sample input face and the EM).

We used different values of transmission of the output coupler (OC) to find the best coupling conditions. The samples were cooled by contact with a copper heat sink, where the sample is soldered with Indium. The copper heat sink has a central window (with 3 mm diameter) to let the laser and pump beams pass through. The samples were joined to the heat sink on the side with the highest doping, whereas the pump beam enters from the side with the lowest doping. This arrangement ensures that the highest power dissipation density occurs on the side nearest to the heat sink.

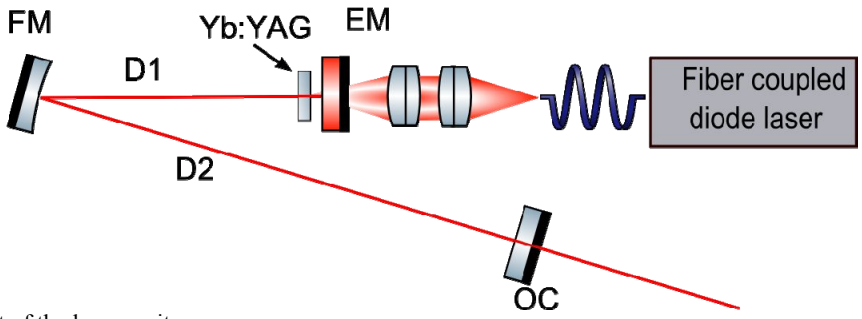

Figure 11. Layout of the laser cavity.

The pump output was modulated with square pulses, at 10 Hz repetition rate (Quasi-Continuous Wave, QCW), and variable duty factors (from 20% to CW). In this way we were able to study the behavior of the samples under different levels of thermal load.

In order to properly evaluate the absorbed pump power in lasing conditions [20]we monitored the power of the residual pump beam transmitted by the sample with an auxiliary power monitor placed behind the folding mirror FM. The correction for the Fresnel reflection at the crystal interfaces was also properly applied.

As the samples absorb different amounts of the available pump power, the comparison between their laser performances is better made considering the absorbed pump power fraction, as it is shown in Figures 12 and 13. The free running lasing wavelength is also reported in the legend of the graphs. The following table reports the slope efficiency (with respect to the absorbed pump power) obtained with different output coupler transmission, under QCW with 20% duty factor. It can be seen that the two samplers with a stepped doping distribution (namely TC-1 and SD-1) show a quite similar slope efficiency under QCW pumping, with a slightly better performance for the sample made by spray drying. Conversely the two samples with graded doping distribution have a lower slope efficiency, in particular in the case of the sample made by spray drying (SD-2).

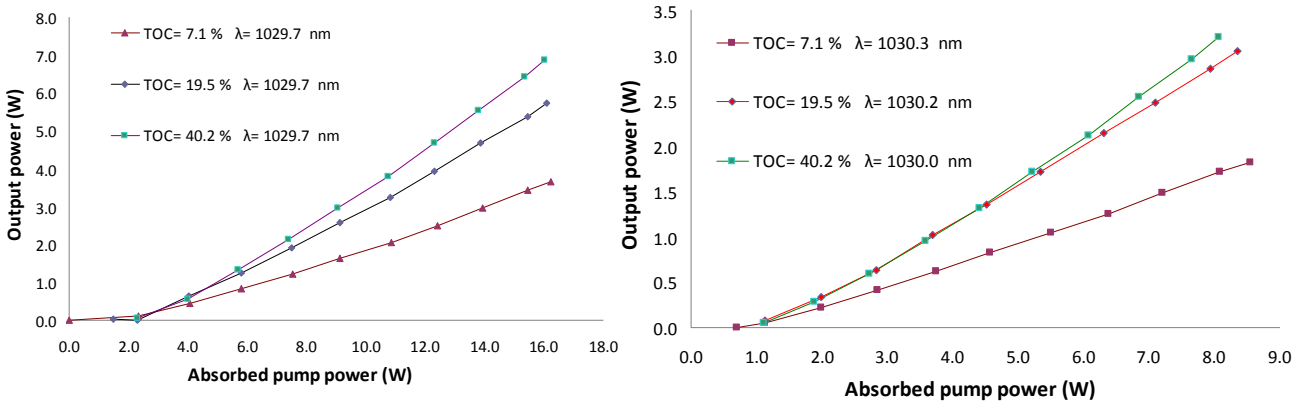

Figure 12. Output power vs. absorbed pump power under QCW pumping conditions, for different values of transmission of the output coupler (TOC). The values of absorbed and emitted power refers to the power on pump phase (i.e. the peak power and not the average power). Left: sample SD-1; right: sample TC-1. Color online.

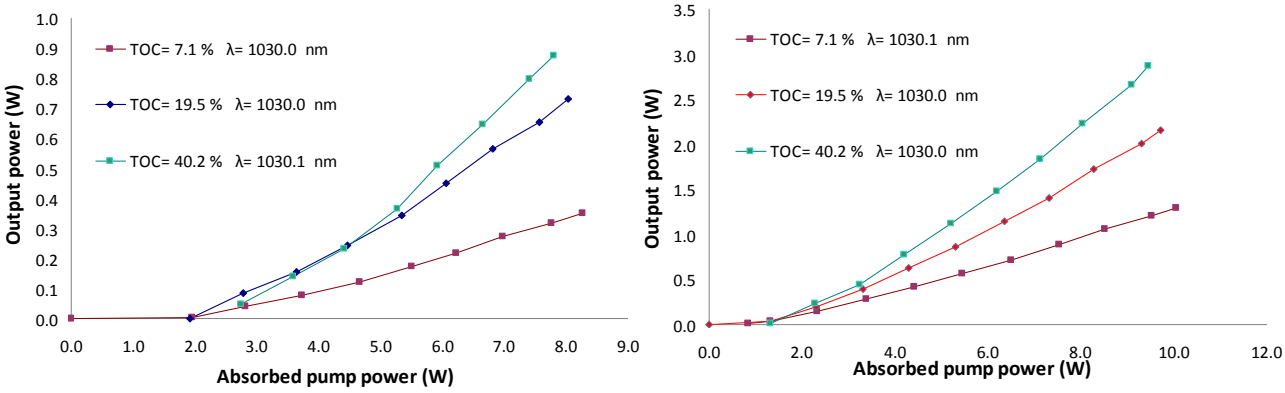

Figure 13. Output power vs. absorbed pump power under QCW pumping conditions, for different values of transmission of the output coupler (TOC). The values of absorbed and emitted power refers to the power on pump phase (i.e. the peak power and not the average power). Left: sample SD-2; right: sample TC-2. Color online.

The behavior of the samples under test was also tested under CW pumping conditions, in order to investigate the effects of an increased thermal load. The results are shown in Figures 14 and 15, and the values of the slope efficiency obtained with the various output couplers are reported in Table 5.

Under CW pumping conditions the samples absorb a slightly higher fraction of the available pump power than in the case of QCW pumping, because the emission wavelength of the pump laser has a slight red shift due to the increased junction temperature. Besides that, it can be seen that the slope efficiency of the sample TC-1 remains substantially constant for all the values of the output coupler transmission, whereas the sample SD-1 with the same doping structure suffers of some decrease in the efficiency. Regarding the samples with graded doping distribution, the sample TC-2 undergoes a slight decrease in the slope efficiency when moving from QCW to CW, whereas the sample SD-2 remains fairly constant, but at a much smaller overall level than the other samples as found in the QCW laser tests.

Table 4. Slope efficiency (with respect to the absorbed pump power) obtained with the various samples with different values of the output coupler transmission, under QCW pumping.

Output coupler transmission	SD-1	TC-1	SD-2	TC-2
7.1	30.0%	25.7%	6.5%	16.1%
19.5	46.9%	43.8%	14.2%	29.9%
40.2	58.1%	52.2%	19.5%	43.8%

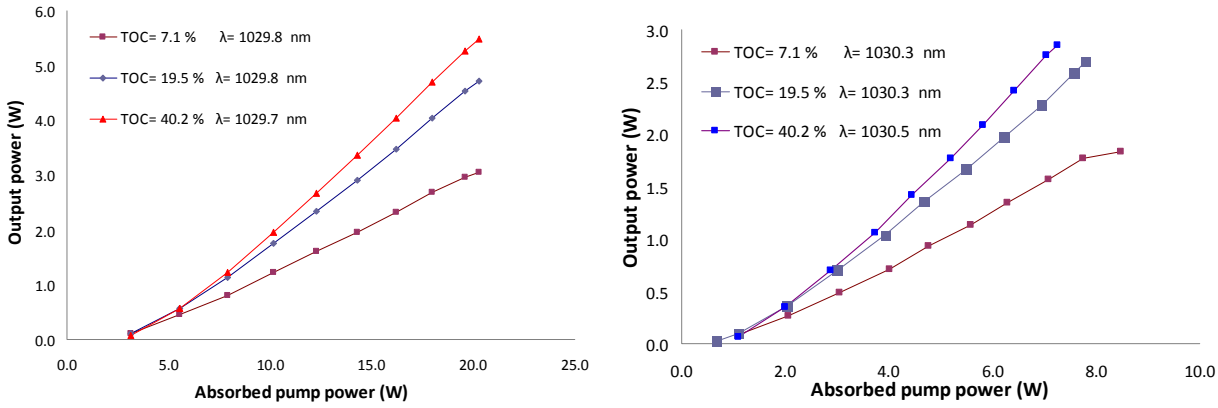

Figure 14. Output power vs. absorbed pump power under CW pumping conditions, for different values of transmission of the output coupler (TOC). Left: sample SD-1; right: sample TC-1. Color online.

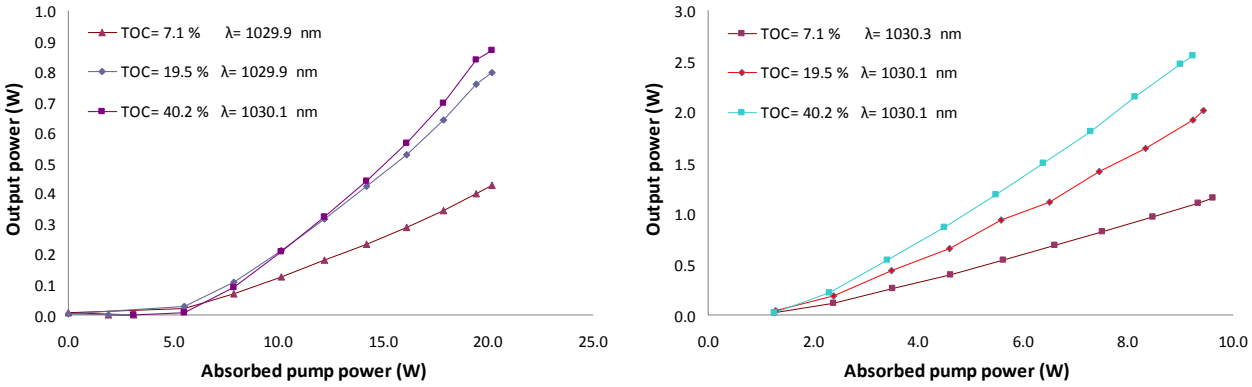

Figure 15. Output power vs. absorbed pump power under CW pumping conditions, for different values of transmission of the output coupler (TOC). Left: sample SD-2; right: sample TC-2. Color online.

Table 5. Slope efficiency (with respect to the absorbed pump power) obtained with the various samples with different values of the output coupler transmission, under CW pumping.

Output coupler transmission (%)	SD-1	TC-1	SD-2	TC-2
7.1	22.6%	25.3%	7.6%	15.5%
19.5	37.3%	44.5%	15.6%	30.1%
40.2	44.2%	54.1%	19.2%	37.4%

5. DISCUSSION AND CONCLUSIONS

The spectroscopic analysis of the samples has confirmed that the absorption and the emission spectra of the Yb in the composite ceramics correspond to those of crystalline Yb:YAG. This indicates that there aren't other optically active phases with absorption or emission in the near IR that can interfere with the laser emission of Yb^{3+}. One of the sample has shown a small residual amount of Y^{2+} due probably to an incomplete annealing procedure, that can be easily fixed.

From the results exposed above, it appears that both the spray drying and the tape cast techniques are capable to produce samples with a quite high laser slope efficiency (around 54-56% for the most favorable output coupling condition), for the two layer doping structure SD-1 and TC-1. This is not in contrast with the fact that the samples made by tape cast show a better overall transmission and uniformity (see section 3) because in the experimental set-up used in the laser test the cross section of the lasing volume of the sample is rather small (the pump beam diameter is about 260 μm), and it is then quite easy to find a defect-free spot whit a high optical quality, with both samples. Indeed the sample made by spray drying (SD-1) has shown a broader point-to-point variability in the laser output than the sample made by tape cast TC-1. This aspect could become an issue if lasing over a broader mode size were required.

At the current level of development the structuring process introduces additional defects, both with the spray drying and with the tape cast technique. This has been evidenced by the test on the optical transmittance uniformity, and substantially confirmed by the results of the laser emission test. The lower efficiency found in the samples SD-2 and TC-2 with respect to the two other samples can be ascribed to the higher value of losses due to internal defects.

Regarding the effects of the thermal load, we can notice that the samples made by tape cast have shown a more stable behavior than the sample made by spray drying. In particular the sample with stepped doping profile (0%-10% Yb, TC-1), shows an almost constant slope efficiency for increasing pump duty factor; conversely the sample made by spray drying with the same doping profile (SD-1) shows a sizeable decrease in slope efficiency when moving from QCW to CW pumping conditions. It is interesting to note that also the sample made by tape casting with 1-3-5-7% doping has a rather stable behavior under increasing thermal load, even though its overall efficiency is affected by the higher density of internal defects.

In conclusion, the results reported here suggest that the tape casting technique is more promising than the spray drying technique for the production of large area gain elements, because at the current level of development it allow to obtain a smaller density of macroscopic defects, which is a clear advantage when large lasing apertures are required. These tests

have also shown that the superimposition of a large number of layers, to create complex doping structures, is susceptible to introduce more defects, probably localized at the interface of the individual layers. Again the tape casting technique seems to be less prone to this detrimental effect than the spray drying technique.

As it has been demonstrated by extensive numerical modeling here and in previous works, the tailoring of the doping distribution is a very powerful method for the reduction of the thermal and thermomechanical effects originated by high intensity laser pumping. The development of ceramics structuring techniques such as those exposed in this paper is a keystone in the attainment of this objective, and will be the subject of future works.

ACKNOWLEDGMENTS

The authors gratefully acknowledge the support from the Italian Ministry of Defence under PNRM, Contract No. 8723 of 19/12/2014 (CeMiLAP).

REFERENCES

[1] DeLoach, L. D., Payne, S. A., Chase, L. L., Smith, L. K., Kway, W. L. and Krupke, W. F., "Evaluation of absorption and emission properties of Yb^{3+} doped crystals for laser applications," IEEE J. Quantum Electron. 29(4), 1179-1191 (1993).

[2] Druon, F., Ricaud, S., Papadopoulos, D. N., Pellegrina, A., Camy, P., Doualan, J. L., Moncorgé, R., Courjaud A., Mottay E., and Georges, P., "On Yb:CaF_2 and Yb:SrF_2: review of spectroscopic and thermal properties and their impact on femtosecond and high power laser performance [Invited]," Opt. Mater. Express **1**(3), 489-502 (2011).

[3] Pirri, A., Toci, G., and Vannini, M., "First laser oscillation and broad tunability of 1 *at.*% Yb-doped Sc_2O_3 and Lu_2O_3 ceramics," Opt. Lett. **36**(21), 4284-4286 (2011).

[4] Pirri, A., Vannini, M., Babin, V., Nikl, M., and Toci, G., "CW and quasi-CW laser performance of 10 *at.*% Yb^{3+}:LuAG ceramic," Laser Phys. **23**(9), 095002-095008 (2013).

[5] Kaminskii, A. A., Akchurin, M. Sh., Gainutdinov, R. V., Takaichi, K., Shirakava, A., Yagi, H., Yanagitani, T., and Ueda, K., "Microhardness and Fracture Toughness of Y_2O_3- and $Y_3Al_5O_{12}$-Based Nanocrystalline Laser Ceramics," Crystallog. Rep. **50**(5), 935-939 (2005).

[6] Esposito, L., Hostaša, J., Piancastelli, A., Toci, G., Alderighi, D., Vannini, M., Epicier, T., Malchère, A., Alombert-Goget, G., and Boulon, G., "Multilayered YAG-Yb: YAG ceramics: manufacture and laser performance," J. Mat Chem. C **2**(47), 10138-10148 (2014).

[7] Koerner, J., Vorholt, C., Liebetrau, H., Kahle, M., Kloepfel, D., Seifert, R., Hein, J., and Kaluza, M. C., "Measurement of temperature-dependent absorption and emission spectra of Yb:YAG, Yb:LuAG, and Yb:CaF_2 between 20 °C and 200 °C and predictions on their influence on laser performance," J. Opt. Soc. Am. B **29**(9), 2493-2502 (2012).

[8] Azrakantsyan, M., Albach, D., Ananyan, N., Gevorgyan, V., and Chanteloup, J.-C., "Yb^{3+}:YAG crystal growth with controlled doping distribution," Opt. Mater. Express **2**(1), 20-30 (2012).

[9] Hostaša J., Esposito L., Biasini V., Piancastelli A., Vannini M., and Toci G., "Layered Yb:YAG ceramics produced by two different methods: processing, characterization and comparison," Proceedings of the SPIE Conference on Solid State Lasers XXV: Technology and Devices, in press (2016)

[10] COSMOS M, Design Star Product, Structural Research and Analysis Corp. – (User's Guide and Tutorial), www.cosmosm.com, Los Angeles (2001)

[11] Ferrara, P., Ciofini, M., Esposito L., Hostaša, J., Labate, L., Lapucci, A., Pirri, A., Toci, G., Vannini, M., and Gizzi L. A., " 3-D numerical simulation of Yb:YAG active slabs with longitudinal doping gradient for thermal load effects assessment," Opt. Express **5**(22), 5375-5386 (2014)

[12] Gaume, R., Viana, B., Vivien, D., Roger, J. P., and Fournier, D., "A simple model for the prediction of thermal conductivity in pure and doped insulating crystals," Appl Phys. Lett. **83**(7), 1355-1357 (2004).

[13] Nikl, M, Yoshikawa, A., and Fukuda, T., "Charge transfer luminescence in Yb^{3+}-containing compounds," Opt. Mater. 26(4), 545-549 (2004)

[14] Henke, M., Perβon, J., and Kuck, S. "Preparation and spectroscopy of Yb^{2+}-doped $Y_3Al_5O_{12}$,$YAlO_3$, and $LiBaF_3$," J. Luminesc. **87-89,** 1049-1051 (2000)

[15] Toci, G., “Lifetime measurements with the pinhole method in presence of radiation trapping: I-theoretical model,“ Appl. Phys. B **106**(1), 63-71 (2011).
[16] Toci, G., Alderighi, D., Pirri, A., and Vannini, M., “Lifetime measurements with the pinhole method in presence of radiation trapping: II-application to Yb3+ doped ceramics and crystals,“ Appl. Phys. B **106**(1), 73-79 (2011).
[17] Kühn, H., Fredrich-Thornton, S. T., Kränkel, C., Peters, R., and Petermann, K., “Model for the calculation of radiation trapping and description of the pinhole method,“ Opt. Lett. **32**(13), 1908-1910 (2007).
[18] Aull, B. F. and Jenssen, H. P., “Vibronic interaction Nd:YAG resulting in non reciprocity of absorption and stimulated emission cross section,“ IEEE J. Quantum Electron. 18(5), 925-930 (1982).
[19] Bruesselbach, H. W., Sumida, D. S., Reeder R. A., and. Byren R. W., "Low-Heat High-Power Scaling Using InGaAs-Diode-Pumped Yb:YAG Lasers," IEEE J. Sel. Top. Quantum Electron. **3**(1), 105-116 (1997).
[20] Pirri, A., Alderighi, D., Toci, G., Vannini, M., Nikl, M., and Sato, H., " Direct Comparison of Yb^{3+}:CaF_2 and heavily doped Yb^{3+}: YLF as laser media at room temperature," Opt. Express, **17** (20), 18312-18319 (2009).